RSC Advances

PAPER

View Article Online
View Journal | View Issue

Cite this: *RSC Adv.*, 2023, **13**, 11697

Acid and alkali-resistant fabric-based triboelectric nanogenerator for self-powered intelligent monitoring of protective clothing in highly corrosive environments

Ting Chen,†[a] Wei-Zhi Song,†[a] Meng Zhang,[a] De-Jun Sun,[a] Duo-Shi Zhang,[a] Chang-Long Li,[a] Wen-Ying Cui,[a] Ting-Ting Fan,[ab] Seeram Ramakrishna [c] and Yun-Ze Long *[ad]

The corrosion of materials severely limits the application scenarios of triboelectric nanogenerators (TENGs), especially in laboratories, chemical plants and other fields where leakage of chemically corrosive solutions is common. Here, we demonstrate a chemical-resistant triboelectric nanogenerator (CR-TENG) based on polysulfonamide (PSA) and polytetrafluoroethylene (PTFE) non-woven fabrics. The CR-TENG can stably harvest biological motion energy and perform intelligent safety protection monitoring in a strong corrosive environment. After treatment with strong acid and alkali solution for 7 days, the fabric morphology, diameter, tensile properties and output of CR-TENG are not affected, showing high reliability. CR-TENG integrated into protective equipment can detect the working status of protective equipment in real time, monitor whether it is damaged, and provide protection for wearers working in high-risk situations. In addition, the nonwoven-based CR-TENG has better wearing comfort and is promising for self-powered sensing in harsh environments.

Received 11th January 2023
Accepted 10th April 2023

DOI: 10.1039/d3ra00212h

rsc.li/rsc-advances

1. Introduction

Human industrial activity drives the modernization process, but it is also prone to accidents in high-risk work environments such as chemical plants,[1] laboratories[2] and special workshops.[3] Of these, leakage or splashing of corrosive solutions such as acid and alkali is the most common event.[1,4] Protective clothing can effectively protect workers in high acid-alkali-hazardous environments, but the common coated protective clothing on the market has problems such as poor air permeability and poor wearing comfort.[5,6] Moreover, when protective clothing is damaged, workers are often unable to perceive it in time, which poses a serious hidden danger to the safety and health of operators.[5,7,8] The wearable triboelectric nanogenerators (TENGs) in self-powered mode can be used for real-time sensing detection, and respond in time when insecurity occurs to prevent danger.[9–13] However, most of the current materials and electrodes of TENGs cannot resist the corrosion of chemical solutions, which may severely limit the work and application scenarios of TENGs.[14–18]

At present, there are few reports about corrosion-resistant TENG. Among them, platinum film[19] and copper–nickel alloy conductive tape[20] have poor air permeability and comfort, so it is not easy to wear or integrate into protective equipment. The polytetrafluoroethylene (PTFE) composite yarn developed by Ma *et al.* solved the problem of electrostatic shedding and successfully applied PTFE material to protective textiles.[1] However, the fabric obtained by the warp and weft weaving method has large pores, and there is a risk of penetration of corrosive chemicals. Therefore, the corrosion-resistant TENG, which is comfortable to wear, has good safety performance and can be integrated into protective equipment for hazard warning and risk reduction, and still needs further researches. As a high-performance fabric, polysulfonamide (PSA) is wear-resistant, durable,[21] flame-retardant,[22–24] excellent in waterproof performance,[25] and has good chemical stability to resist corrosion.[26–28] Therefore, this material is suitable for protective equipment such as protective clothing and protective gloves in special environments.[21] Here, we prepared PSA nonwovens by using needle-free wire electrode electrospinning equipment. PSA materials obtained by electrostatic spinning technology not only retain its own advantages of hydrophobic, corrosion resistant and chemical stability, but also wear comfort, have good air permeability, which had the potential to produce or integrate into protective equipment. In

[a]*Collaborative Innovation Center for Nanomaterials & Devices, College of Physics, Qingdao University, Qingdao 266071, China. E-mail: yunze.long@163.com; yunze.long@qdu.edu.cn; Tel: +86 139 5329 0681*

[b]*Industrial Research Institute of Nonwovens & Technical Textiles, College of Textiles & Clothing, Qingdao University, Qingdao 2266071, China*

[c]*Center for Nanofibers & Nanotechnology, National University of Singapore, Singapore*

[d]*State Key Laboratory of Bio-Fibers & Eco-Textiles (Qingdao University), Qingdao 266071, China*

† These two authors contributed equally to this work.

the preparation process, needle-free wire electrode electrospinning equipment was used, that can not only provides sufficient high voltage to ensure the stability of the spinning process, but also overcomes the problem of low efficiency of traditional wet spinning,[29] and can efficiently produce materials for industrial and commercial applications. In addition, pure PSA spinning solution has the difficulty of poor spinnability, and we solved this problem by using a small amount of thermoplastic polyurethane (TPU) as the auxiliary polymer of the solution.

In this work, we combined PSA fabrics with nanogenerators and developed a chemically stable frictional electric nanogenerator (CR-TENG). The device had a short-circuit current of 250 nA and an open-circuit voltage of 26 V. After testing, TENG's material can resist corrosion of strong acid and strong alkali solution for up to 7 days. Meanwhile, the TENG output remained stable after various degrees of corrosion (from pH = 3 to pH = 11) and under different temperature working environment. Moreover, CR-TENG can monitor human motion status while working stably in harsh environments, and can be integrated into protective equipment for self-powered safety monitoring. This TENG overcomes the impact of environmental corrosion on the material and enables self-powered sensing applications in locations with harsh operating environments, risk and hidden dangers such as security monitoring.

2. Experimental section

2.1 Materials

PSA (Mw = 15 000, solid content of 15%) was purchased from Shanghai Tianlong Fiber Co., Ltd. TPU (Germany BASF 1180A, Mw = 10 000, njection molding) was purchased from Shanghai Duo Yuan Plastic Materials Co., Ltd. PTFE concentrated dispersion (concentration 60%, PTFE particle size is about 200 nm, Mw = 100.016), polyvinyl alcohol (PVA, 1788 type, Mw = 44.05) powder was purchased from Shanghai Aladdin Chemical Co., Ltd. *N*,*N*-Dimethylacetamide (DMAC, 99%, Mw = 87.12) was purchased from China Sinopharm Chemical Reagent Co., Ltd.

2.2 Preparation of friction material

12 wt% PSA spinning solution was obtained by dispersing purchased PSA solution and a small amount of TPU solid in DMAc solution after continuous stirring. A needle-free wire electrode electrospinning apparatus as shown in Fig. 1e was used. During the preparation process, the spinning voltage was set to a positive high voltage of 28 kV and a negative high voltage of 28 kV, the spinning distance was 150 mm, and the moving speed of the conductive gauze of the substrate was 5 m min^{-1}.

The PVA powder was dissolved in ionized water, heated in a water bath at 50 °C until the dissolution was complete, and then a 10% PVA solution was obtained. The PVA–PTFE spinning solution was obtained after mixing the PVA solution and the PTFE solution at a volume ratio of 1 : 1. The positive and negative voltages of the equipment were both set to 18 kV, and the spinning distance was 150 mm to prepare PVA–PTFE films. The dried PVA–PTFE fiber membrane was placed in a muffle furnace and heated to 360 °C at a rate of 3 °C min^{-1}, and then naturally cooled to room temperature after holding for a period of time to obtain a sintered PVA–PTFE (S-PVA–PTFE) composite membrane.

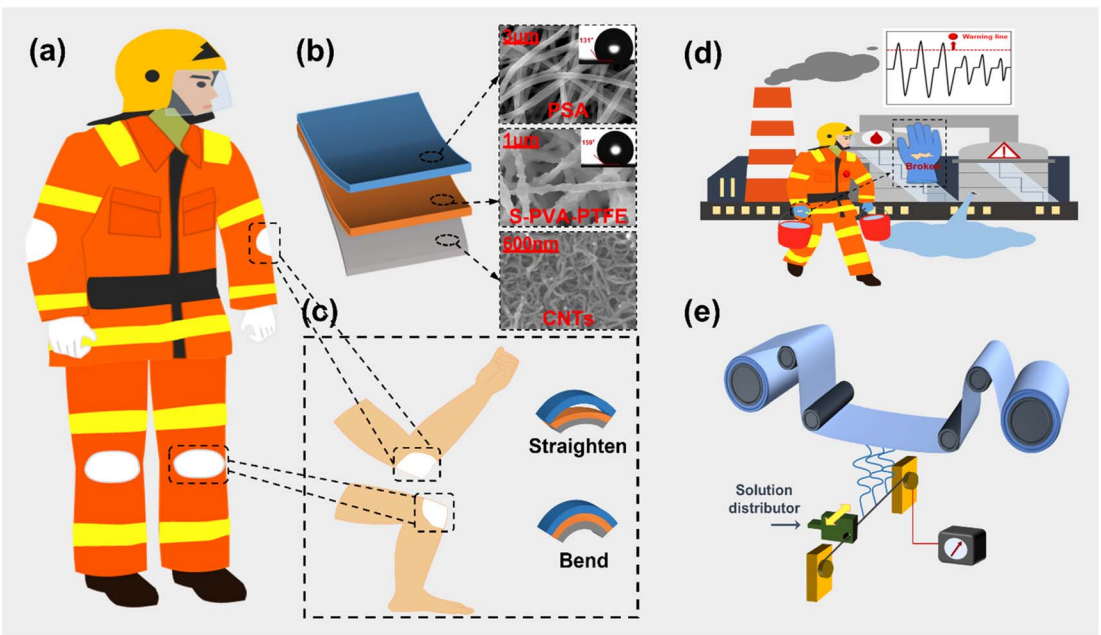

Fig. 1 Schematic diagram of CR-TENG and intelligent chemical protective clothing. (a) Schematic diagram of the chemical protective suit integrated with CR-TENG in the part with large bending activity. (b) CR-TENG's structure and SEM image. (c) Working mode of the CR-TENG integrated at the joint. (d) Application scenarios of the chemical protective suit composed of CR-TENG. (e) Schematic diagram of the needle-free wire electrode electrospinning.

CNTs electrodes were obtained by mixing 1.0 g of carbon nanotubes (CNTs), 0.2 g of polyacrylic acid aqueous solution (50 wt%), and 18.8 g of deionized water together, and then ultrasonic treatment at a power of 150 W for 1 h.

The above spinning process was carried out on the conditions of relative humidity of 55 ± 5% and temperature of 25 ± 5 °C.

2.3 Characterization

The surface morphologies of the materials were characterized by scanning electron microscopy (SEM, TM-1000, Hitachi and Sigma 500 field emission). The contact separation process test was performed with a linear motor (Beijing Nano, R-LP3) and a stepper motor. Electrical signal output of the TENG was measured through an oscilloscope (KEYSIGHT DSO-X 3024T) and a current amplifier (SR570). The mechanical properties of the films were investigated using a universal strength tester (Instron 6025, Jinan Liangong Testing Technology Co., Ltd).

3. Result and discussion

3.1 CR-TENG

In this work, we developed a chemical-resistant CR-TENG. This single-electrode working mode TENG is composed of PSA, sintered PVA–PTFE (S-PVA–PTFE) and carbon nanotube coating electrode with excellent chemical stability and electrical conductivity, and its structure is shown in Fig. 1b. Among them, PSA material (contact angle 131°) and S-PVA–PTFE material (contact angle 159°) have excellent waterproof performance. In addition, after sintering, the acid and alkali resistance and electrical performance of PVA–PTFE material are improved.[30] The carbon nanotube coating as the electrode not only has excellent flexibility,[31] but also ensures the stability of the electrical output.[32] As shown in Fig. 1a, TENG can be integrated into human joints (*e.g.* elbows and knees) and gloves. The CR-TENG fixed on the elbow and knee joints, as shown in Fig. 1c, continuously contacts and separates with the movement of the joints, and the electrical signals are outputted to monitor human movement dynamically. In addition, the smart glove composed of CR-TENG can not only collect hand motion energy to detect hand movement status, but also automatically cause an alarm when the working state of the glove is in danger in real time, as shown in Fig. 1d. This self-powered protective glove with safety monitoring feature helps protect operators working in high-risk areas. To prepare the friction layer material, we used an electrospinning device with a needle-free wire electrode (Fig. 1e). The equipment can manufacture fiber membranes on a large scale, and can realize the industrial production and application of electrospinning fabrics.

3.2 Working mechanism of CR-TENG

In the single-electrode TENG, the PSA loses electrons better than S-PVA–PTFE, so after contact, the surface of PSA has a positive potential, while the surface of S-PVA–PTFE loses electrons and has a negative potential. The working mechanism of CR-TENG is shown in Fig. 2a. Due to the contact electrification effect, when PSA fabric and S-PVA–PTFE material contact under the action of external force, as shown in Fig. 2a(i), charge transfer occurs on the surfaces of the two non-woven fabrics, and equal and opposite charges are induced. When the external force is unloaded, as shown in Fig. 2a(ii), the two contact surfaces are separated from each other. In order to balance the static electricity, the charge is directed from the carbon nanotube electrode to the ground. As shown in Fig. 2a(iii), when the two materials are separated to the maximum extent, the charge will stop flowing. At this time, the resulting potential difference and the corresponding current reach the peak. When PSA approaches S-PVA–PTFE again, the charge moves from the ground to the carbon nanotubes, and the whole process is reversed (as shown in Fig. 2a(iv)). The two fabrics repeat the

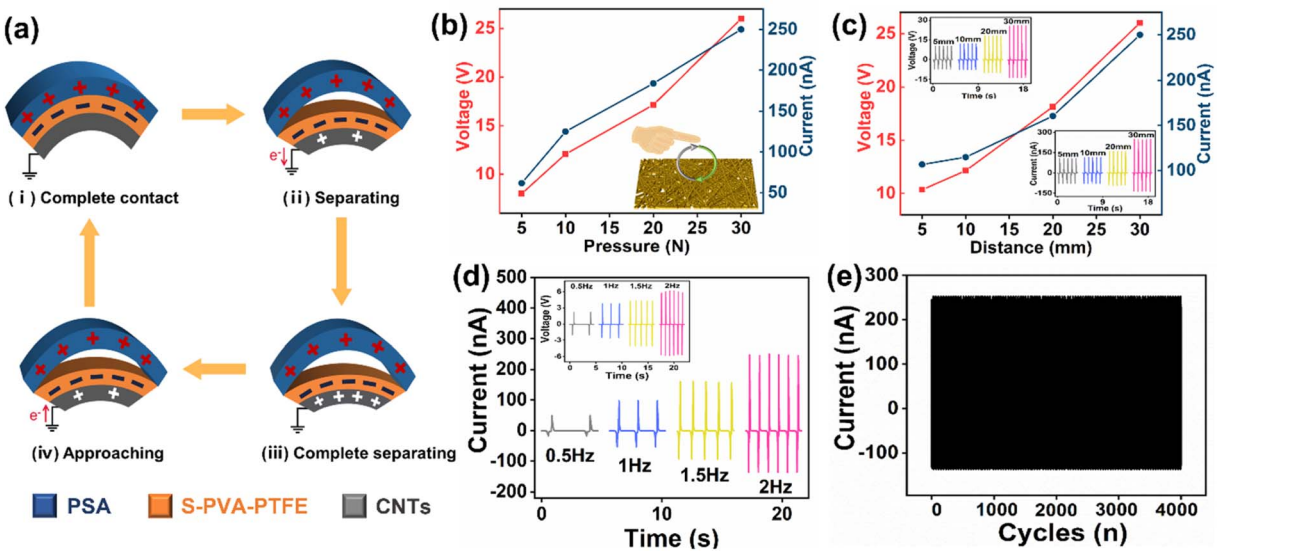

Fig. 2 Triboelectric performance of CR-TENG. (a) Schematic illustration of working mechanism of CR-TENG. Output of CR-TENG at different pressures (b), distances (c) and frequencies (d). (e) Durability and stability testing of CR-TENG.

process of contact and separation, continuously outputting alternating current.

3.3 Electrical output performance of CR-TENG

To study the triboelectric properties, a CR-TENG composed of PSA (40 mm × 50 mm) material and S-PVA–PTFE (30 mm × 30 mm) material was designed to harvest mechanical energy in the environment. When the temperature was 24 °C and the humidity was 55%, the method of controlling variables was used to evaluate the adaptability of TENG to different environments. As shown in Fig. 2b, when the impact force changes, the greater the force, the more contact between the two friction layers, the current and the voltage increase accordingly. When the distance between the friction layers increases, as shown in Fig. 2c, the electrical output also rises. When the impact force and distance are constant, the current output of TENG increases with the increase of the impact frequency, as shown in Fig. 2d. This is mainly due to the shorter duration of the current peak at higher impulse frequencies, resulting in larger short-circuit currents. Accordingly, the open-circuit voltage improves as the frequency increases. The maximum current (250 nA) and voltage (26 V) were obtained when the impact frequency was 2 Hz, the impact force was 30 N and the distance between the two friction layers was 30 mm.

Durability and long-term stability are important indexes to judge whether TENG can be practically applied. At constant frequency, pressure, and friction spacing, 4000 contact-separation cycles were tested on CR-TENG. During the cycling process, the current signal does not have obvious deletion and reduction, as shown in Fig. 2e, and the CR-TENG exhibits excellent persistence and output stability.

3.4 Performance of CR-TENG after acid and alkali-base treatments

The hydrophobicity of PSA and S-PVA–PTFE was tested by dipping method. The two non-woven fabrics were immersed in methyl orange solution for a certain period of time and then taken out (Fig. 3a). The surfaces of the two materials were not dyed and discolored, and no liquid remained on the surface. Both friction materials have excellent water resistance. In order to test the anti-corrosion performance of CR-TENG, the possibility of its application in severe environments, especially in strong acid and alkali conditions, was confirmed. First, after immersing the PSA composite membrane and the S-PVA–PTFE fiber membrane in strong acid and strong alkali solutions for 10 min, it was found that the surfaces of the materials were not damaged (Fig. 3b). To study the chemical durability of PSA and S-PVA–PTFE. We treated the two materials in 36% concentrated hydrochloric acid and 1 mol L^{-1} sodium hydroxide solution for 7 days. After taking out and drying, the microstructure was characterized by scanning electron microscope, and the change in the microstructure of the comparative materials were observed and the fabric diameter transformations were analyzed.

The SEM images in Fig. 3c(i)–(iii) show that the PSA films immersed in two corrosive solutions for a long time did not suffer from dissolution and curling, and the fibers did not find any abnormality such as breakage. Fig. 3c(iv) shows the fiber diameter distribution before and after corrosion of PSA non-woven fabrics. The fiber diameters of PSA fabrics without chemical corrosion are mainly (51.28%) in the 125–160 nm range, while 56.28% and 54.45% of PSA fibers treated with strong acid and strong alkali are distributed between 125–160 nm, respectively. There was no reduction in the fiber diameter. Similarly, it can be found that the S-PVA–PTFE nonwovens soaked in 36% concentrated hydrochloric acid and 1 mol L^{-1} sodium hydroxide for 7 days did not dissolve or partially dissolve, nor did they break, bend, or pit, as shown in Fig. 3d(i)–(iii). As shown in Fig. 3d (iv), the particle size distribution shows that the diameter distribution range of S-PVA–PTFE fibers before and after corrosion is mainly concentrated between 210–300 nm (72.56% untreated, 75% after strong acid treatment, 69% after strong alkali treatment). There was no obvious change in fiber diameter before and after material treatment, showing excellent corrosion resistance.

FTIR spectra were tested and analyzed to further support the chemical resistance of the materials. As shown in Fig. 3e, PSA materials before and after corrosion all have stretching vibration absorption peaks of N–H bond in amide at 3337 cm^{-1}, which is one of the characteristic peaks of PSA. And they all have the stretching vibration peak of –C=C– of benzene ring at 1530 cm^{-1} and the symmetric stretch peak of sulfone group (–SO_2–) at 1150 cm^{-1}.[33] For S-PVA–PTFE, Fig. 3f shows the characteristic absorption peaks of C–F at 617 cm^{-1} and C–O at 1125 cm^{-1} existed before and after chemical treatment.[34] FTIR analysis proved that neither of the two materials showed shrinkage or deviation of characteristic peak value after chemical corrosion. In addition, air permeability affects the wearing comfort of materials. We tested the permeability of PSA materials before and after corrosion. As shown in Fig. 3g, the PSA material can achieve air permeability of 18.23 mm s^{-1}. At the same time, the air permeability of PSA material after strong acid and base treatment remained stable, and did not decrease. Through the softness test, it was found that both materials showed good flexibility, as shown in the Fig. 3h. Good air permeability and flexibility can ensure the wearing comfort.

Through the above observation and research, both materials were found to have excellent chemical stability and corrosion resistance. Based on –SO_2– groups, PSA materials have excellent chemical stability. During the sintering process of the PVA–PTFE film, the PTFE dissolves and completely wraps the surface of the PVA fiber.[30] The S-PVA–PTFE composite film has excellent acid and alkali resistance and corrosion resistance. The chemical structures of PSA and S-PVA–PTFE materials are shown in Fig. 4a. Fig. 4b shows that the tensile strain of PSA changed slightly after being etched by strong acid solution (42% to 45%); the tensile strain of the PSA nonwoven treated with strong alkali solution is almost unchanged, and the stress decreases slightly. The tensile stress–strain of the sintered PVA–PTFE material changed slightly after being treated with two corrosive solutions, as shown in Fig. 4c. It can be seen that the two fabric materials after severe corrosion still maintain a certain stability, tensile ability and deformation ability.

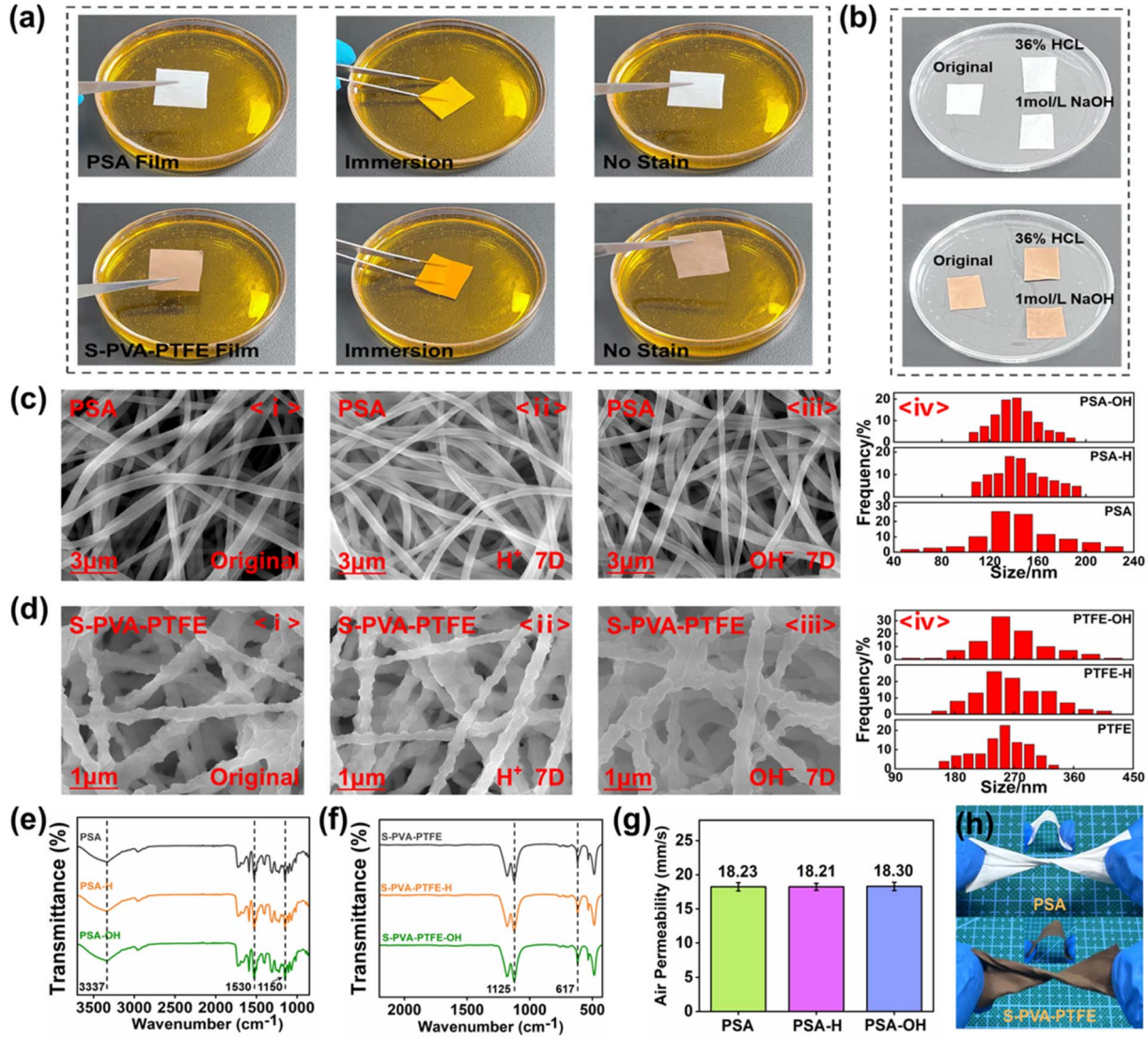

Fig. 3 Macroscopic and microscopic comparison after acid and alkali treatment. (a) The process diagram of PSA composite membrane and S-PVA–PTFE composite membrane immersed in methyl orange solution. (b) Optical photos of PSA and S-PVA–PTFE before and after acid–base treatment. (c) SEM image of the PSA material untreated and treated in 36% hydrochloric acid and 1 mol L^{-1} sodium hydroxide solution for 7 days, and the fiber diameter distribution before and after treatment. (d) SEM image of S-PVA–PTFE material untreated and treated with concentrated hydrochloric acid and sodium hydroxide solution for 7 days, and the fiber diameter distribution of fibers before and after treatment. (e) and (f) are FTIR analysis of PSA and S-PVA–PTFE materials before and after corrosion, respectively. (g) Air permeability test of PSA materials before and after chemical treatment. (h) Softness test of the materials.

In order to study the resistance of CR-TENG to different degrees of corrosion, PSA and sintered PVA–PTFE were treated with solutions of different pH values (pH = 3, pH = 5, pH = 7, pH = 9, and pH = 11), as shown in Fig. 4d. When controlling variables, the test compared the changes of current and voltage before and after corrosion. Fig. 4e shows that the current output of TENG after corrosion in different pH solutions is almost unchanged, and only slightly decreases at pH = 3 and pH = 11. The voltage of TENG did not change significantly under different degrees of corrosion, as shown in Fig. 4f. After being treated with highly acidic (pH = 3, as shown in Fig. 4g) and alkaline (pH = 11, as shown in Fig. 4h) solutions, the output of CR-TENG is stable during the 4000 operating cycles with no significant loss of signal. The electrical performance of CR-TENG remains stable under different degrees of corrosion, and TENG has strong environmental adaptability and stability.

In addition, the CR-TENG was subjected to different temperature operating environments in order to study the sensitivity of its output to temperature. As shown in Fig. 4i, under operating conditions of 25 °C, 35 °C, 45 °C and high temperature 55 °C, the current output of the developed TENG remains stable and does not rise or fall. The temperature adaptability of the TENG provides conditions for its steady working under high temperature environment.

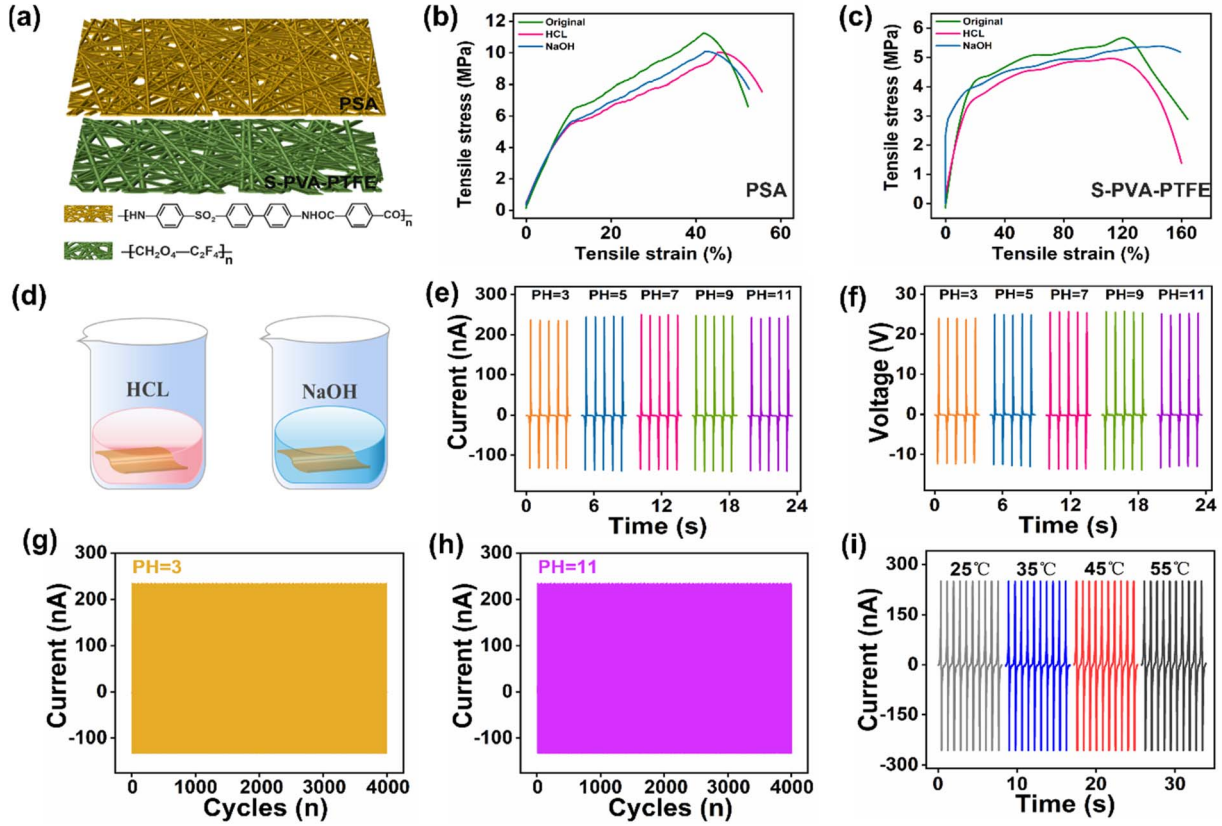

Fig. 4 Performance testing in harsh environment. (a) Chemical structures of PSA and S-PVA–PTFE. (b) Tensile stress–strain curves of the PSA film before and after corrosion. (c) Tensile stress–strain curves of S-PVA–PTFE membrane before and after corrosion. (d) Schematic diagram of the treatment of the film in an acid–base environment. (e) Short current and (f) voltage of CR-TENG treated with solutions of different pH values. (g) and (h) are 4000 cycles of current of CR-TENG after strong acid and strong alkali treatment respectively. (i) Output current of the TENG at different temperatures.

3.5 CR-TENG for biological motion monitoring

An arched CR-TENG was designed as shown in Fig. 5a(i), and integrated it into a glove to develop a smart glove. As shown in Fig. 5a, when the finger touches the CR-TENG on the palm, a negative voltage signal is generated; when the finger is removed, a positive output is generated; when the finger is stationary, no signal is generated. CR-TENG has the function of reflecting its own working state, as shown in Fig. 5b. When touched, an intact CR-TENG that is not damaged generated obvious electrical signals; however, after the PSA friction layer was destroyed, the TENG output signal decreased. In addition, nitrile gloves fixed with CR-TENG realized the intelligent self-powered detection of hand movement. This may be because the damaged friction layer hinders the transfer of electrons. We designed different gestures and described these gestures with different numbers, as shown in Fig. 5c. Fig. 5d shows the real-time voltage signals collected by bending different fingers sequentially. When hand gestures of "4-0-1-2-3-4" were carried out in sequence as shown in the above picture, finger contact caused contact and separation of the corresponding CR-TENG, and corresponding electrical signals were generated to record finger movements trajectory. TENG exhibits excellent gesture detection and recognition capabilities. The CR-TENG also showed a sensitive response to major joint movements, such as at the elbows and knees. As shown in Fig. 5e, as the elbow is straightened and bent at a certain rate, the PSA and S-PVA–PTFE continuously friction with each other to produce a stable and repeatable voltage output. In addition, the CR-TENG can also be fixed on the wearer's knee to further record the activities of the knee, as shown in Fig. 5f. The developed CR-TENG which can monitor its own working state has outstanding biological motion sensing ability and stable signal output. CR-TENG realizes accurate detection of human joint motion by identifying sensing signals, and it can be further superimposed on the flexible and easily bendable parts of the chemical protective equipment to track and detect the movement trajectory of workers in high-risk environment.

3.6 Intelligent security protection monitoring

In order to enable the corrosion-resistant TENG with self-powered sensing mode for further applications in high-risk environment. We designed a smart protective glove, the outer layer of the glove is PSA non-woven fabric and the inner layer is S-PVA–PTFE material coated with CNTs, as shown in Fig. 6a. Wearing protective gloves with corrosion resistance and real-time motion monitoring functions, as shown in Fig. 6b, can effectively prevent the corrosion and injury of splashed or leaked acid–base liquids to the staff. Moreover, the continuous

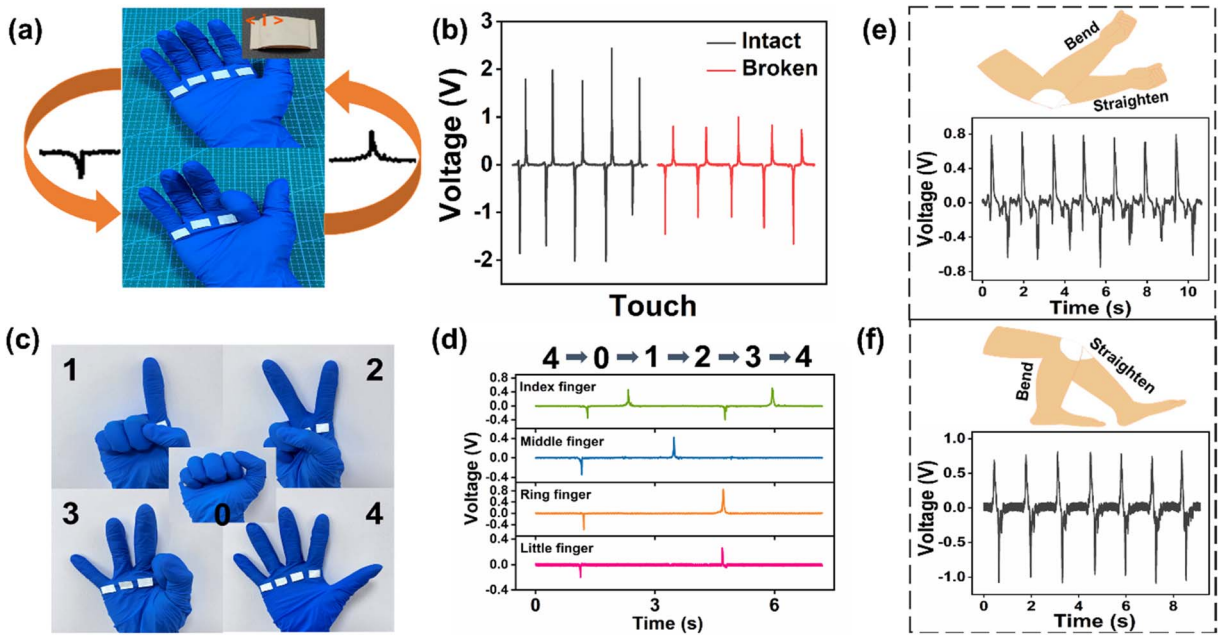

Fig. 5 CR-TENG detects human motion. (a) Physical image of the CR-TENG at the joint and its photograph for monitoring hand motion. (b) Output voltage of intact and damaged CR-TENG. (c) Different gestures and their corresponding numbers. (d) The output signal in sequence when the finger moves "4-0-1-2-3-4". (e) Elbow movement and output during movement. (f) Knee activity and output during activity.

friction between the two materials realizes the dynamic monitoring of the movement of the worker's hand during the operation.

The CR-TENG in the glove can also detect and sense the working state of the protective glove in real time through the change of the output. Through research and comparison, it can

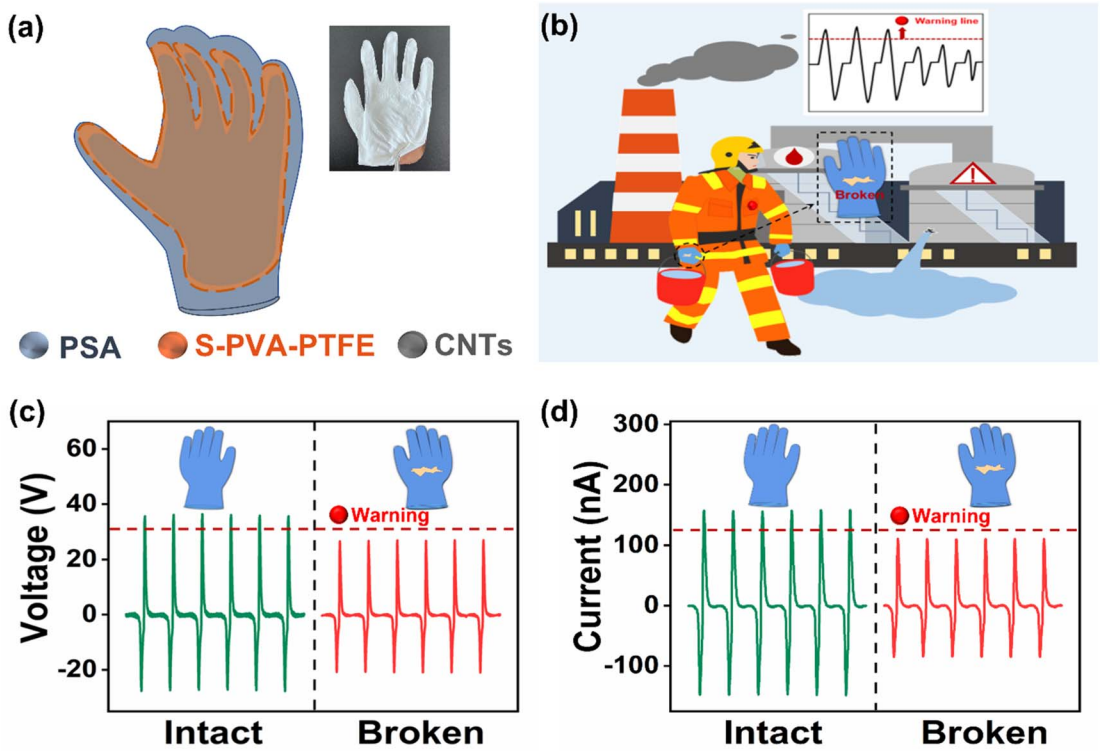

Fig. 6 Application of CR-TENG in the intelligent chemical protective clothing system. (a) Structural drawings of the protective glove. (b) Application scenario diagram. (c) Voltage output before and after glove breakage. (d) Current output before and after glove breakage.

be found that, as shown in Fig. 6c, the output voltage of the intact glove is 37 V during use, and the output drops to 27 V when damaged. Likewise, the intact glove produced a current of 159 nA, while the broken glove current output showed a clear downward trend, as shown in Fig. 6d. When the electrical signal drops below a certain value, an alarm will be triggered to indicate that the gloves are damaged, and it should be replaced in time. Observing the change of output during the use of the gloves can help us clearly realize the working status of the gloves. This smart protective glove can detect the integrity of the chemical protective clothing in real time and remind users to change it in time to prevent chemical injuring to their hands. CR-TENG is expected to be further combined with protective gear such as protective clothing for intelligent safety monitoring in high-risk environments.

4. Conclusion

In conclusion, a chemical-resistant TENG was developed using PSA non-woven fabrics and S-PVA–PTFE membranes. The stability of the device in harsh environment and the reliability of output under different degrees of corrosion were verified. The designed TENG has three functions: acid and alkali corrosion resistance, dynamic monitoring of human movement and automatic safety protection monitoring. The protective glove based on CR-TENG can monitor the integrity of itself in real time, ensuring the personal safety of the staff. The developed TENG can be further laminated on the easily bendable and damaged parts of the chemical protective clothing, and response to joint movement and safety. This chemical-resistant TENG can realize self-powered intelligent sensing while meeting the requirements of wearing comfort, and has broad application prospects in harsh high-risk corrosion environment.

Conflicts of interest

There are no conflicts to declare.

Acknowledgements

This work was supported by the National Natural Science Foundation of China (51973100 and 52273077), the State Key Laboratory of Bio-Fibers & Eco-Textiles, Qingdao University (RZ2000003334 and ZDKT202108), and Shandong Province Introduction of Top Talents (Team) “One Thing, One Discussion” (DC1900013728).

References

1 L. Y. Ma, R. H. Wu, A. Patil, J. Yi, D. Liu, X. W. Fan, F. F. Sheng, Y. F. Zhang, S. Liu, S. Shen, J. Wang and Z. L. Wang, Acid and Alkali-Resistant Textile Triboelectric Nanogenerator as a Smart Protective Suit for Liquid Energy Harvesting and Self-Powered Monitoring in High-Risk Environments, *Adv. Funct. Mater.*, 2021, **31**(35), 2012963–2102974.

2 A. D. Menard and J. F. Trant, A review and critique of academic lab safety research, *Nat. Chem.*, 2020, **12**(1), 17–25.

3 Z. W. Mo, S. H. Lu and M. Shao, Volatile organic compound (VOC) emissions and health risk assessment in paint and coatings industry in the Yangtze River Delta, China, *Environ. Pollut.*, 2021, **269**, 115740–115750.

4 B. Wang, D. L. Li and C. Wu, Characteristics of hazardous chemical accidents during hot season in China from 1989 to 2019: A statistical investigation, *Saf. Sci.*, 2020, **129**, 104788–104798.

5 H. Zhou, H. X. Wang, H. T. Niu, A. Gestos and T. Lin, Robust, Self-Healing Superamphiphobic Fabrics Prepared by Two-Step Coating of Fluoro-Containing Polymer, Fluoroalkyl Silane, and Modified Silica Nanoparticles, *Adv. Funct. Mater.*, 2013, **23**(13), 1664–1670.

6 Y. Xu, J. L. Sheng, X. Yin, J. Y. Yu and B. Ding, Functional modification of breathable polyacrylonitrile/polyurethane/TiO_2 nanofibrous membranes with robust ultraviolet resistant and waterproof performance, *J. Colloid Interface Sci.*, 2017, **508**, 508–516.

7 A. H. Sajatovic, S. F. Grgac and D. Zavec, Investigation of Flammability of Protective Clothing System for Firefighters, *Materials*, 2022, **15**(7), 2384.

8 H. L. He, J. R. Liu, Y. S. Wang, Y. H. Zhao, Y. Qin, Z. Y. Zhu, Z. C. Yu and J. F. Wang, An Ultralight Self-Powered Fire Alarm e-Textile Based on Conductive Aerogel Fiber with Repeatable Temperature Monitoring Performance Used in Firefighting Clothing, *ACS Nano*, 2022, **16**(2), 2953–2967.

9 W. H. Wang, J. Y. Zhou, S. Wang, F. Yuan, S. Liu, J. S. Zhang and X. L. Gong, Enhanced Kevlar-based triboelectric nanogenerator with anti-impact and sensing performance towards wireless alarm system, *Nano Energy*, 2022, **91**, 106657.

10 Z. W. Ren, X. Liang, D. Liu, X. J. Li, J. F. Ping, Z. M. Wang and Z. L. Wang, Water-Wave Driven Route Avoidance Warning System for Wireless Ocean Navigation, *Adv. Energy Mater.*, 2021, **11**(31), 210116–210126.

11 J. Y. Chang, H. Meng, C. S. Li, J. M. Gao, S. Q. Chen, Q. Hu, H. Li and L. Feng, A Wearable Toxic Gas-Monitoring Device Based on Triboelectric Nanogenerator for Self-Powered Aniline Early Warning, *Adv. Mater. Technol.*, 2020, **5**(5), 1901087.

12 G. Q. Gu, C. B. Han, Y. Bai, T. Jiang, C. He, B. D. Chen and Z. L. Wang, Particle Transport-Based Triboelectric Nanogenerator for Self-Powered Mass-Flow Detection and Explosion Early Warning, *Adv. Mater. Technol.*, 2018, **3**(6), 180009–180016.

13 H. J. Qiu, W. Z. Song, X. X. Wang, J. Zhang, Z. Y. Fan, M. Yu, S. Ramakrishna and Y. Z. Long, A calibration-free self-powered sensor for vital sign monitoring and finger tap communication based on wearable triboelectric nanogenerator, *Nano Energy*, 2019, **58**, 536–542.

14 Z. Zhou, P. Wang, J. W. Li, C. Y. Wang, J. H. Chen, L. Y. Zhu, H. T. Zhu and D. Zhang, A self-powered microbiosensor system for specific bacteria detection based on triboelectric nanogenerator, *Nano Energy*, 2022, **98**, 107317–107329.

15 C. Y. Wang, P. Wang, J. H. Chen, L. Y. Zhu, D. Zhang, Y. Wan and S. Y. Ai, Self-powered biosensing system driven by triboelectric nanogenerator for specific detection of Gram-positive bacteria, *Nano Energy*, 2022, **93**, 106828–106839.

16 X. M. Zhang, J. Hu, Q. X. Zeng, H. K. Yang, W. C. He, Q. Y. Li, X. C. Li, H. M. Yang, C. G. Hu and Y. Xi, A Non-Encapsulated Polymorphous U-Shaped Triboelectric Nanogenerator for Multiform Hydropower Harvesting, *Adv. Mater. Technol.*, 2021, **6**(7), 2001199–2991208.

17 W. X. Sun, N. Luo, Y. B. Liu, H. Li and D. A. Wang, A New Self-Healing Triboelectric Nanogenerator Based on Polyurethane Coating and Its Application for Self-Powered Cathodic Protection, *ACS Appl. Mater. Interfaces*, 2022, **14**(8), 10498–10507.

18 Y. G. Feng, Y. B. Zheng, Z. U. Rahman, D. A. Wang, F. Zhou and W. M. Liu, Paper-based triboelectric nanogenerators and their application in self-powered anticorrosion and antifouling, *J. Mater. Chem. A*, 2016, **4**(46), 18022–18030.

19 W. Lu, Y. Xu, Y. X. Zou, L. A. Zhang, J. S. Zhang, W. T. Wu and G. F. Song, Corrosion-resistant and high-performance crumpled-platinum-based triboelectric nanogenerator for self-powered motion sensing, *Nano Energy*, 2020, **69**, 104430–104439.

20 K. Q. Xia, Z. W. Xu, Z. Y. Zhu, H. Z. Zhang and Y. Nie, Cost-Effective Copper-Nickel-Based Triboelectric Nanogenerator for Corrosion-Resistant and High-Output Self-Powered Wearable Electronic Systems, *Nanomaterials*, 2019, **9**(5), 9700–9712.

21 M. Wang and J. Li, Thermal protection retention of fire protective clothing after repeated flash fire exposure, *J. Ind. Text.*, 2016, **46**(3), 737–755.

22 K. J. Wu, J. C. Yu, J. Q. Yang, S. H. Chen, X. F. Wang, Y. M. Zhang and H. P. Wang, Properties and phase morphology of cellulose/aromatic polysulfonamide alloy fibers regulated by the viscosity ratio of solution, *Cellulose*, 2018, **25**(2), 903–914.

23 L. P. Yue, J. J. Zhang, Z. H. Liu, Q. S. Kong, X. H. Zhou, Q. Xu, J. H. Yao and G. L. Cui, A Heat Resistant and Flame-Retardant Polysulfonamide/Polypropylene Composite Nonwoven for High Performance Lithium Ion Battery Separator, *J. Electrochem. Soc.*, 2014, **161**(6), A1032–A1038.

24 Z. M. Wei, Z. F. Wu, Q. Su, C. R. Zhu, H. Y. Zeng, X. J. Wang, S. R. Long and J. Yang, A novel high-performance and outstanding flame retardancy polysulfonamide nanofibrous filter for the high-efficiency PM2.5 filtration, *Sep. Purif. Technol.*, 2022, **287**, 120355.

25 Z. G. Zhu, L. L. Zhong, Y. Wang, G. F. Zeng and W. Wang, Mechanically durable biomimetic fibrous membrane with superhydrophobicity and superoleophilicity for aqueous oil separation, *Chin. Chem. Lett.*, 2020, **31**(10), 2619–2622.

26 M. He, T. Yuan, W. J. Dong, P. Li, Q. J. Niu and J. Q. Meng, High-performance acid-stable polysulfonamide thin-film composite membrane prepared via spinning-assist multilayer interfacial polymerization, *J. Mater. Sci.*, 2019, **54**(1), 886–900.

27 G. Bargeman, Recent developments in the preparation of improved nanofiltration membranes for extreme pH conditions, *Sep. Purif. Technol.*, 2021, **279**, 119725.

28 Y. J. Li, D. Yuan, Q. Geng, X. Yang, H. Z. Wu, Y. Z. Xie, L. M. Wang, X. Ning and J. F. Ming, MOF-Embedded Bifunctional Composite Nanofiber Membranes with a Tunable Hierarchical Structure for High-Efficiency PM0.3 Purification and Oil/Water Separation, *ACS Appl. Mater. Interfaces*, 2021, **13**(33), 39831–39843.

29 X. Yang, Y. Pu, S. X. Li, X. F. Liu, Z. S. Wang, D. Yuan and X. Ning, Electrospun Polymer Composite Membrane with Superior Thermal Stability and Excellent Chemical Resistance for High-Efficiency PM2.5 Capture, *ACS Appl. Mater. Interfaces*, 2019, **11**(46), 43188–43199.

30 J. P. Wu, W. Liang, W. Z. Song, L. N. Zhou, X. X. Wang, S. Ramakrishna and Y. Z. Long, An acid and alkali-resistant triboelectric nanogenerator, *Nanoscale*, 2020, **12**(45), 23225–23233.

31 M. Su, J. Brugger and B. Kim, Simply Structured Wearable Triboelectric Nanogenerator Based on a Hybrid Composition of Carbon Nanotubes and Polymer Layer, *Int. J. Precis. Eng. Manuf. Green Technol.*, 2020, **7**(3), 683–698.

32 H. Wang, M. Y. Shi, K. Zhu, Z. M. Su, X. L. Cheng, Y. Song, X. X. Chen, Z. Q. Liao, M. Zhang and H. X. Zhang, High performance triboelectric nanogenerators with aligned carbon nanotubes, *Nanoscale*, 2016, **8**(43), 18489–18494.

33 Y. J. Li, J. F. Ming, D. Yuan and X. Ning, High-Temperature Bearable Polysulfonamide/Polyurethane Composite Nanofibers' Membranes for Filtration Application, *Macromol. Mater. Eng.*, 2021, **306**(7), 8.

34 T. Zhang, Z. Hu, J. Yu, L. Chen, J. Zhu and Q. Wang, Research progress in PTFE fiber manufacturing technology, *Synth. Fiber Ind.*, 2012, **35**(3), 36–43.